Progress in Physics of Applied Materials 2 (2022) 103–112

Semnan University

Progress in Physics of Applied Materials

journal homepage: https://ppam.semnan.ac.ir/

Impact of Nano-Micro Particle Size on Structural, Magnetic, and Electrical Properties of $La_{0.5}Ca_{0.5}MnO_3$ Manganites

N. Modaresi, P. Kameli*

Department of Physics, Isfahan University of Technology, Isfahan, 84156-83111, Iran.

ARTICLE INFO

Article history:
Received: 8 November 2022
Revised: 21 November 2022
Accepted: 17 December 2022

Keywords:
Manganites
Resistivity
Thermal hysteresis
Sintering Temperature

ABSTRACT

Structural, magnetic, and electrical properties of $La_{0.5}Ca_{0.5}MnO_3$ samples prepared at two different sintering temperatures (800°C and 1350°C which were labeled S800 and S1350, respectively) have been investigated. The Reitveled refined XRD patterns indicate an orthorombic structure with P*nma* space group for both samples. Ac susceptibility measurements show that, the fraction of ferromagnetic and antiferromagnetic phases could be controlled with sintering temperature. S800 sample has a ferromagnetic state while the antiferromagnetic phase is enhanced in S1350 sample which causes the increase of thermal hysteresis in this sample. Two distinct regions ($T>\Theta_D/2$ and $T<\Theta_D/2$, Θ_D is the Debye's temperature) were noticed to investigate the electrical properties. Based on the resistivity data at $T>\Theta D/2$ region, the S800 and S1350 samples follow the adiabatic and non-adiabatic small polaron hopping (SPH) models, respectively. At $T<\Theta_D/2$ region, the 3-dementional variable range hopping (VRH) model displays a good correlation with the experimental data of both samples. The related parameters of both SPH and VRH models are extracted. The results show that these parameters are particle size dependent.

1. Introduction

Over past years, manganites of general formula $R_{1-x}A_xMnO_3$ (R= trivalent rare earth ion and A= divalent alkaline earth ion) have attracted much attention due to their marvelous features including colossal magnetoresistance (CMR), magnetic, and electrical transport properties [1-4]. Among different perovskite manganites, $La_{0.5}Ca_{0.5}MnO_3$ manganite has been extensively studied because it displays interesting properties such as charge, orbital, and spin ordering states [5-9].The bulk sample of $La_{0.5}Ca_{0.5}MnO_3$, first undergoes paramagnetic (PM) to ferromagnetic metallic (FM) transition below $T_c\sim240$ K and subsequently charge ordered antiferromagnetic (CO-AFM) insulating occurs below $T_N\sim120$ K upon cooling process [6, 8].

The strong coulomb interaction among electrons on the same Mn ion leads to the charge ordering [10]. The PM to FM transition is second order and the FM to CO-AFM transition is first order with thermal hysteresis [11]. However, it is favorable for the system to form an inhomogeneous state consisting of distinct FM and CO-AFM phases at low temperatures. Also it has been found that lower sintering temperature in $La_{0.5}Ca_{0.5}MnO_3$ system leads to a FM state and in spite of bulk samples, the FM phase is developed and charge ordering (CO) is destroyed in nano-sized samples of $La_{0.5}Ca_{0.5}MnO_3$ [5].

It is well-known that sintering temperature and particle size play a key role in magnetic and electrical transport properties of manganites, So that, the magnetic and transport properties of nanostructured samples are not similar to those of bulk ones [5, 6, 12]. For instance, it is reported that the magnetization, Curie temperature (T_c), and electrical resistivity (ρ) decrease with increasing particle size in $La_{0.67}Ba_{0.33}Mn_{0.9}Cr_{0.1}O_3$ manganite [13]. In addition T_c doesn't change significantly, while metal-insulator transition temperature (T_{MI}) is affected by particle size in $La_{0.7}Ca_{0.3}MnO_3$ [14]. Kuberkar et al. have found the reduction of resistivity by increasing particle size and improving crystallinity in $La_{0.7}Ca_{0.3}MnO_3$ and $Nd_{0.7}Sr_{0.3}MnO_3$ nanostructured manganites [15]. As a matter of fact, electrical studies revealed that the density of grain boundaries can extremely affect the electrical properties of nanostructured materials [16-18].

* Corresponding author. Tel.: +98 3113913756
E-mail address: kameli@cc.iut.ac.ir

DOI: 10.22075/ppam.2022.28929.1037

Usually the reduction of particle size causes a monotonically increase in the resistivity of manganites because of the high density of grain boundaries [15, 19]. But in addition to the effect of grain size, the AFM state at low temperatures is also important in the resistivity behavior of half doped manganites ($R_{0.5}A_{0.5}MnO_3$). As an example, Levy et al. have found that the resistivity of the $La_{0.5}Ca_{0.5}MnO_3$ samples increases by increasing grain size at low temperatures because of the induction of AFM phase at low temperatures which can overcome the effect of grain size[6].

Although double-exchange interaction can basically explain the conduction mechanism in ferromagnetic-metallic region of manganites, however, more useful mechanisms, such as charge/orbital ordering [20-23], phase separation and small polaron correlated transport [24, 25] are needed to explain other features of these broad set of materials. Small polaron hopping (SPH) and variable range hopping (VRH) models are suggested to explain the resistivity of manganites in nonmetallic regime [26-29]. Polaron is used to understand the interactions among electrons and atoms in a solid material. The polaron could be "Large" or "small" which depends on comparable values of polaron radius and lattice constant. Actually the radius of a large polaron is larger than lattice constant and it is the opposite in a small polaron. The electron is confined to a volume of one-unit cell or less in small polaron. Also large polaron has tendency to band-like electrical transport, while small polaron undergoes hopping electrical transport. In order to investigate the conductivity mechanism in samples, all temperature ranges were separated into two ones: $T>\Theta_D/2$ and $T<\Theta_D/2$ (Θ_D is the Debye's temperature) where different kinds of mechanisms are followed. In $T>\Theta_D/2$, the SPH model is responsible and in $T<\Theta_D/2$, the VRH model is followed [27, 29].

Up to now, different manganites have been investigated by these theoretical models [13, 26, 27, 29], but it seems that less attention has been paid to the $La_{0.5}Ca_{0.5}MnO_3$ manganites. In this work, the $La_{0.5}Ca_{0.5}MnO_3$ samples were prepared at two different sintering temperatures, 800˚C and 1350˚C and their structural, magnetic, and electrical properties have been investigated. Particularly, the resistivity data of the samples are fitted to different models and the impact of particle size was investigated.

2. Experimental

Polycrystalline micrometer and nanometer-sized samples of $La_{0.5}Ca_{0.5}MnO_3$ were synthesized by a simple method which is based on the grinding of nitrate/acetate precursors in the presence of citric acid. Lanthanum acetate, calcium nitrate, manganese acetate, and citric acid with 99.9% purity were used as starting materials. The powders were weighted in appropriate proportions and mixed in a planetary ball mill for 135 minutes. The ball-milled powders were calcined at 600°C. Finally, the resulting powders were sintered at 800°C and 1350°C for 5 hours which were labeled S800 and S1350, respectively. The structural characterization of obtained samples was carried out by X-ray diffraction (XRD) spectroscopy using Philips (X'PERT) X-ray diffractometer with Cu-Kα (λ=0.154 nm) radiation. The refinement method of Rietveld was revealed by Fullprof package. The microstructures of the samples were analyzed by field emission scanning electron microscope (FE-SEM) using Hitachi FE-SEM (model S-4160). The magnetic properties were estimated by temperature dependence of ac susceptibility using a Lake Shore 7000 susceptometer. The electrical transport properties were investigated by temperature dependence of resistivity using a Leybold closed cycle refrigerator.

3. Results and discussion

3.1. Structural properties

The Reitveled refinement was carried out for samples using Fullprof program [30], in which the XRD patterns of the experimental data are compared with the calculated results. Figure 1 shows Reitveled refined XRD patterns of samples. In XRD pattern of samples, no trace of secondary phase was observed. It is evaluated that the samples don't have any detectable impurity. Based on the XRD refinement, formation of orthorhombic structure with P*nma* space group was confirmed for samples.

The crystal data of the samples such as lattice parameters and their respective unit cell volumes were extracted. It was found that the lattice volume cell is around 224 $Å^3$ and 223 $Å^3$ for S800 and S1350 samples, respectively. The reduction of lattice volume cell could be due to the Johan-Teller (JT) distortion of MnO_6 octahedron and to the variation of $\Theta_{Mn\text{-}O\text{-}Mn}$ [13].

The surface morphology was revealed by FE-SEM and Figure 2 shows typical FE-SEM images of the S800 and S1350 samples. It is to be noted that the average grain size increases from nanometer range to the micrometer range by increasing sintering temperature from 800 ˚C to 1350 ˚C.

3.2 Magnetic properties

In order to study the effect of particle size on the magnetic phase transitions, ac magnetic susceptibility λ(T) versus temperature was measured at an ac field of 1 mT and frequency of 333 Hz upon cooling and warming processes, as shown in Figure 3. It is observable that S800 sample shows typical features of a PM-FM (at T_C∼270 K) reversible system without any signature of CO in all temperature ranges. On the other hand, S1350 sample shows PM-FM transition at T_C∼240 K, the slight reduction of λ(T) at T_{CO}∼205 K, indicates the presence of CO and the drastic decline in values of λ(T) at T_N∼120 K on cooling curve and T_N∼180 K on the warming one is due to the AFM transition. The transition temperatures were obtained from dλ/dT curves which can be seen in the inset of Figure 3. The tendency of FM phase in nanostructured $La_{0.5}Ca_{0.5}MnO_3$ samples is also reported by others [6]. As it was discussed before, the well-known CO state was not found in S800 sample. It has been reported that in $La_{0.5}Ca_{0.5}MnO_3$ samples, the CO state is suppressed when the particle size is reduced less than 180 nm and it is completely destroyed in less than 15 nm nanoparticles [31, 32].

Based on the observed magnetic behavior, the Figures 4 were proposed to explain the effects of particle size and

temperature on the phase coexistence in $La_{0.5}Ca_{0.5}MnO_3$ manganite. Figures 4(a)-4(c) show the different phases at various temperatures in the bulk sample. The system

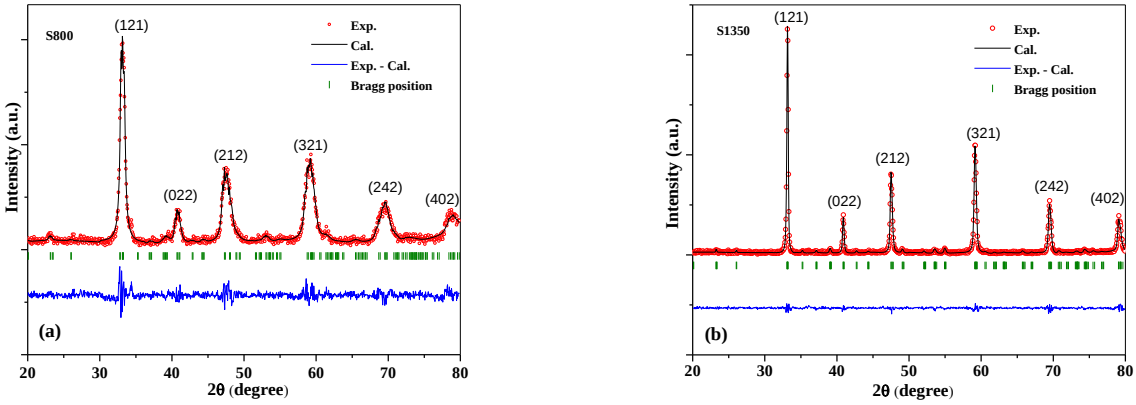

Fig. 1. XRD pattern refinements using Fullprof software for XRD patterns of $La_{0.5}Ca_{0.5}MnO_3$samples sintered at different temperatures, (a) S800 and (b) S1350 (*red circle;* experimental data, *upper black solid line;* calculated pattern, *lower blue solid line;* subtracted pattern, and Bragg positions are shown as *small green bars*).

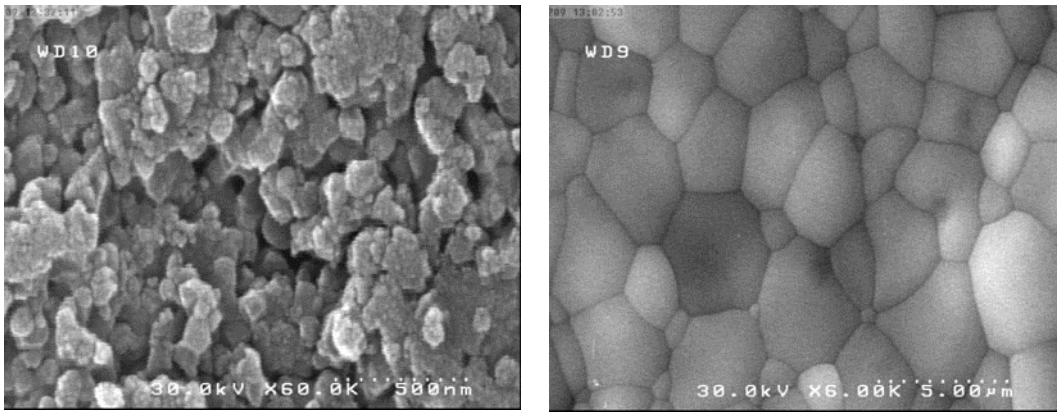

Fig. 2. Typical FE-SEM images of (a) S800 and (b) S1350 samples.

undergoes FM transition at temperature region of $T_{CO}<T<T_c$ (see Fig. 4(a)), after that CO-AFM phase nucleate and develop slowly by decreasing temperature (see Fig. 4(b)).The CO-AFM phase grow rapidly by further decrease of temperature (see Fig. 4(c)) and the coexistence of FM and CO-AFM phases can be seen below Nèel temperature (T_N). The Figures 4(d)-4(f) display the corresponding behavior of nanoparticles. As it is shown in these figures, the PM phase converts to the FM one by decreasing temperature, so that, the FM phase is the dominant one at low temperatures (see Fig. 4(f)). Also it can be seen in Figures 4 that the CO state is suppressed by decreasing particle size. As a matter of fact, the CO state is not significant in nano-sized sample, so only the FM behavior is observed in λ(T) curve of this sample.

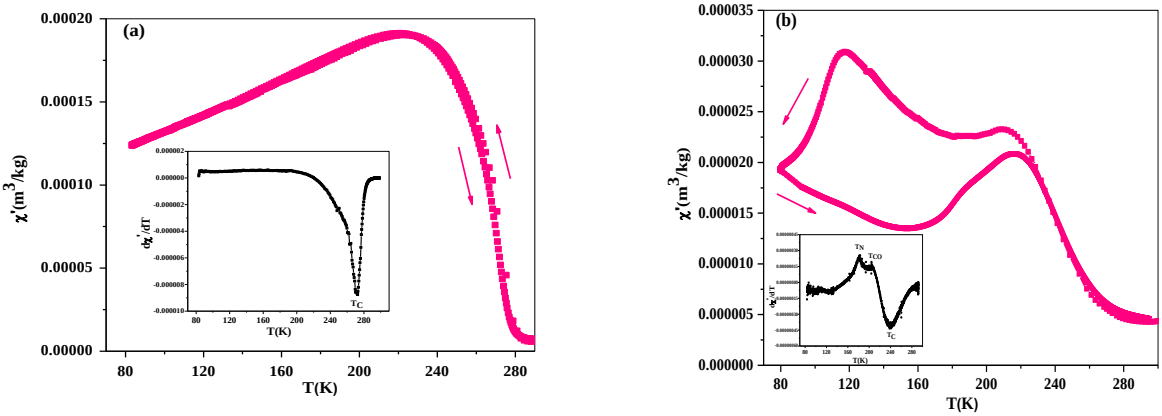

Fig. 3. Temperature dependence of the real part of ac susceptibility (in a field of 1 mT and at a frequency of 333 Hz), for samples of (a) S800 and (b) S1350. The arrows indicate the direction of cooling and warming processes. The insets show the first derivative of the real part of ac susceptibility upon heating process for samples.

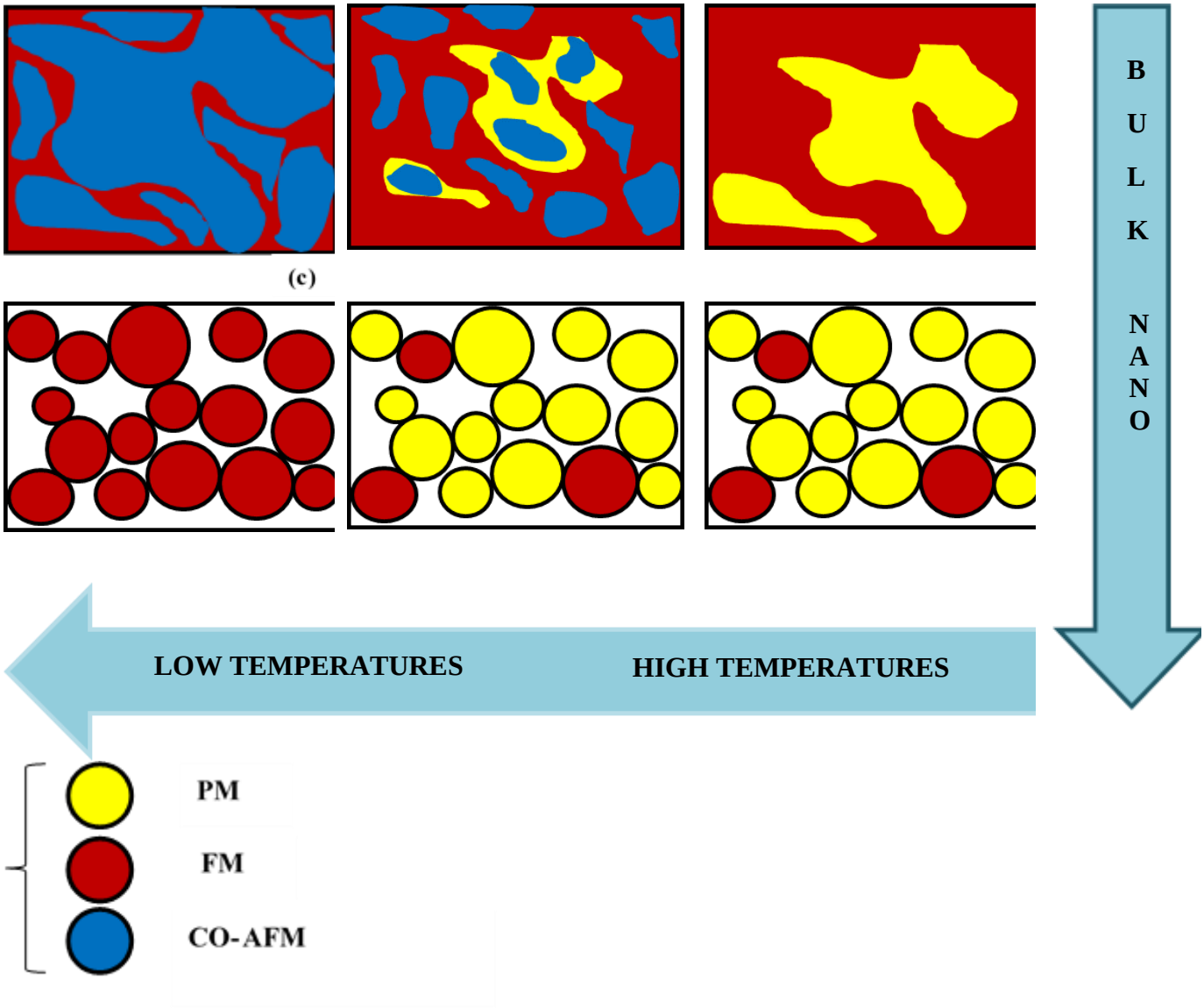

Fig. 4. Proposed configuration of different phases (PM: yellow, FM: red and CO-AFM: blue) at various temperature regions in bulk and nano-sized samples. Figs. 4(a)-4(c) for bulk samples ((a): temperature range of $T_{CO}<T<T_C$, (b): temperature range of $T_N<T<T_{CO}$ and (c): temperature region of $T<T_N$). Figs. 4(d)-4(f) for nano-sized samples at temperature region of $T<T_C$.

Different reasons such as the effect of uncompensated spins on the surface of nanostructured samples and variation in oxygen content could be responsible for the difference between the magnetic properties of samples with different particle sizes[5, 6, 12, 33, 34].

It is to be noted in Figure 3 that the S1350 sample displays a typical feature of irreversible system and it shows thermal hysteresis. In contrast, almost no thermal hysteresis was observed in S800 sample. It is well-known that the thermal hysteresis is a signature of first order phase transition and confirms the coexistence of CO-AFM and FM phases in system.

It is reported that thermal hysteresis originates from lattice distortion, phase separation, martensitic mechanism, magnetoelastic energy, and lattice strains [5, 35-38]. Also it is found that the pining of domain walls by lattice defects can lead to thermal hysteresis [39]. As it was mentioned above, the S1350 sample tends to CO-AFM below TN~120 K upon cooling process, but there are still few FM clusters in system at low temperatures and the coexistence of FM and AFM phases cause a large thermal hysteresis in S1350 sample. It is also reported that the CO-AFM domains are more strained than the FM ones [40, 41]. Actually, the system tends to FM phase at low temperatures by decreasing sintering temperature, so the interfacial elastic energy and lattice strains reduce in system and it causes a reduction in the width of thermal hysteresis by decreasing sintering temperature. Particle size and sintering temperature play a key role in phase separation and thermal hysteresis in phase separated manganites[5, 6].

3.3 Electrical transport property

The electrical transport is probably the most interesting physical property of the manganites. The temperature dependence of electrical resistivity of the samples is shown in Figure 5. It is obvious that the resistivity of both samples increases significantly by decreasing temperature ($d\rho/dt <0$), so these samples show insulator-like behavior within our experimental limits. Figure 5 also shows that the

resistivity increases with sintering temperature at low temperatures (below ~200 K), so the resistivity of S1350 sample is larger than that of S800 sample. Also, it is remarkable to note that, the rate of resistivity enhancement in S1350 sample is higher than that of S800 sample by decreasing temperature at low temperatures. In contrast, at high temperature region (T>~200 K) the resistivity increases by decreasing sintering temperature (see the inset of Fig. 5) and the resistivity of S800 sample is larger than that of S1350 sample at this temperature region. This behavior could be explained on the basis of grain size effects [18, 42-45]. Two kinds of conduction channels could be considered in polycrystalline manganites. One is related to intragrain and the second one to intergrain hopping of the conduction electron between the neighboring sites. As it was discussed before, the grain size decreases and the grain boundary density increases with decreasing sintering temperature, this leads to the enhancement of charge carriers scattering at grain boundaries. As a matter of fact, grain boundaries are naturally less crystalline and non-magnetic, so the increase of grain boundary density causes the weakening of double-exchange mechanism. Based on the magnetic analysis, the AFM phase is the dominant one in S1350 sample at low temperatures. In contrast, the S800 sample shows FM behavior with more grain boundaries at low temperatures. Both dominant AFM phase at low temperatures in S1350 sample and large density of grain boundaries in S800 sample, cause the increase of resistivity in these systems. It seems that the effect of AFM phase on resistivity of S1350 sample is more than the effect of grain boundaries on the resistivity of S800 sample. This causes the larger resistivity in S1350 sample than in S800 sample at low temperatures. At higher temperatures (T>~200 K), the FM phase is the dominant one in S1350 sample, so the resistivity of S800 sample is more than of the S1350 one due to the large density of grain boundaries in S800 sample.

In order to investigate the most suitable conduction mechanism in $La_{0.5}Ca_{0.5}MnO_3$ manganites, the all temperature ranges were separated into two regions: $T>\Theta_D/2$ and $T<\Theta_D/2$ (Θ_D is the Debye's temperature). We focused our attention on these two regions.

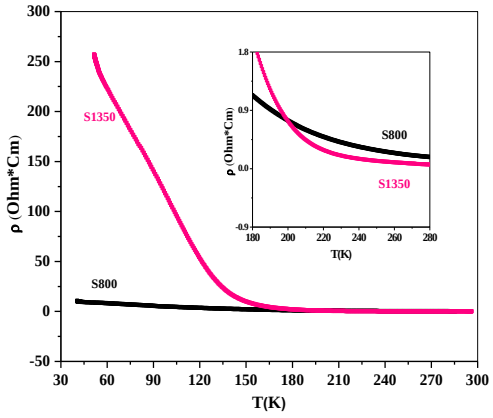

Fig. 5. Temperature dependence of the resistivity for S800 and S1350 samples.The inset shows high temperature resistivity behavior.

3.3.1. T> $\Theta_D/2$: Small Polaron Hopping (SPH) model

The conductivity of samples at $T>\Theta_D/2$ can be explained using small polaron hopping (SPH) conduction mechanism. In this model, a polaron is assumed to be trapped inside a local energy well of height E_a (activation energy) and some parameters such as an applied electric field can lower a side of the well slightly with respect to the other one, this situation helps the polaron to hop more in that direction [46].The polaronic models could be either adiabatic or non-adiabatic approximations. In adiabatic hopping, the electron is relaxed in the potential well of its lattice distortion all the time but in non-adiabatic hopping, the electron jumps out the potential well and then the lattice moves to be balanced with the electron new position. According to these mechanisms, the temperature dependence of resistivity (ρ) is expressed as [47, 48]:

$$\rho = \rho_\alpha T \exp\left(\frac{E_a}{K_B T}\right) \quad \text{(adiabatic)} \qquad (1)$$

$$\rho = \rho_\alpha T^{3/2} \exp\left(\frac{E_a}{K_B T}\right) \quad \text{(non-adiabatic)} \qquad (2)$$

Where E_a is activation energy, K_B is Boltzman's constant, and ρ_α is residual resistivity. First of all, the Θ_D should be estimated from the plot of $Ln(\rho/T)$ and $Ln(\rho/T^{3/2})$ versus $(1/T)$ (Fig. 6). The $\Theta_D/2$ values were obtained from the temperature where the linearity of Figure 6 disappears in the high-temperature region. Θ_D has been found to be 444 K and 450 K for S800 and S1350 samples, respectively. The Θ_D values and their increasing trend with increasing sintering temperature are similar to previous reports about manganites [29, 49, 50].

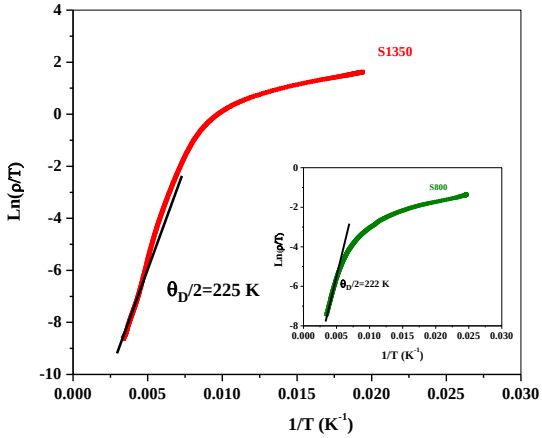

Fig. 6. Variation in $Ln(\rho/T)$ as a function of $(1/T)$ for S1350 sample. The inset shows $Ln(\rho/T)$ versus $(1/T)$ for S800 sample.

It is important to find conduction in our samples is governed by adiabatic or non-adiabatic models. The plot of $Ln(\rho/T)$ and $Ln(\rho/T^{3/2})$ versus $(1/T)$ were drawn

separately for both samples, as it is shown in Figures 7(a) and 8 (a). Also, the data of high temperature region ($T > \Theta_D/2$) were selected and fitted by adiabatic and non-adiabatic models for both samples, as it is shown in Figures 7(b) and 8 (b). The related parameters are evaluated and given in Table 1. The activation energy (E_a) is determined from the slope of $Ln(\rho/T)$ and $Ln(\rho/T^{3/2})$ versus $(1/T)$ plots above $\Theta_D/2$. It is notable that the linear correlation coefficient (R^2) of both adiabatic and non-adiabatic models are almost the same for each sample and it is difficult to distinguish the nature of hopping mechanism in this temperature region by this analysis. To further elucidate the nature of hopping mechanism, one has to check the necessary conditions for using either mechanism. Holstein's relation also confers the nature of hopping conduction [51]. The Holstein restriction is established on supposing that polaron bandwith (J) can be treated as a perturbation in the corresponding Schrodinger equation. According to the Holstein's relation, J should satisfy the following conditions:

$$\text{SPH model} \begin{cases} J > \emptyset & \text{for adiabatic polaron} \\ J < \emptyset & \text{for non-adiabatic} \end{cases}$$

Where $\emptyset$ is expressed as:

$$\phi = \left(\frac{2k_B T E_a}{\pi}\right)^{\frac{1}{4}} \left(\frac{h\nu_{Ph}}{\pi}\right)^{\frac{1}{2}} \quad (3)$$

And the J value can be estimated by approximating the equation for high temperature jump site [19, 27]:

$$J \cong 0.67 h\nu_{Ph} \left(\frac{T}{\theta_D}\right)^{\frac{1}{4}} \quad (4)$$

Where ν_{ph} in both above equations is the optical phonon frequency which is estimated from the equations of $h\nu_{ph}=K_B\theta_D$ and T=300 K.

The J and Ø values were estimated and tabulated in Table 2. It is reported that the $J < E_a/3$ is the condition for the formation of small polaron, otherwise there will be large polaron [51].

Since $J < E_a/3$ for both samples, it can be concluded that SPH model is responsible for the conduction mechanism of both samples.

It is also shown in Table 2 that the $\emptyset$ value was obtained to be 22.86 meV (for S800 sample) and 24.55 meV (for S1350 sample. Also, the J value was estimated to be 23.25 meV for S800 sample and 23.48 meV for S1350 sample. Since $J > \emptyset$ for S800 sample and $J < \emptyset$ for S1350 sample, this leads to conclude that the transport properties are dominated by adiabatic and non-adiabatic SPH models for S800 and S1350 samples, respectively. Consequently, it is evident that the value of E_a increases from 111.53 meV for S800 sample to 156.09 meV for S1350 sample and ρ_α decreases from $6.41\times10^{-6}\Omega CmK^{-1}$ to $2.22\times10^{-8}\Omega CmK^{-1}$ for S800 and S1350 samples, respectively.The E_a values are nearly close to the reported ones for other perovskite manganites [29,52]. The reduction of E_a value by decreasing particle size may be attributed to the localization of charge carriers that hop between the Mn^{3+} to Mn^{4+} sites through double exchange mechanism which occurs only if the two moments are parallel. The reduction of residual resistivity with sintering temperature is in consistant with the resistivity data at high temperatures (see the inset of Fig5.). This reduction could be due to the better quality of crystal structure, phase purity, and larger grain size of S1350 sample than S800 one.

Now we can estimate some physical parameters such as small polaron coupling constant (γ_p) which is a criterion to measure the electron-phonon interaction in manganites. It follows the relation [53, 54]:

$$\gamma_p = \frac{2E_a}{h\nu_{ph}} \quad (5)$$

Also the polaron mass (m_p) and rigid lattice effective mass (m^*) are given by the following relation [53, 54]:

$$\mathbf{m_p} = \left(\frac{\mathbf{h^2}}{\mathbf{8\pi^2 JR^2}}\right) \mathbf{exp}(\boldsymbol{\gamma_p}) = \mathbf{m^* exp}\ (\boldsymbol{\gamma_p}) \quad (6)$$

γ_p and $\frac{m_p}{m^*}$ values were estimated and listed in Table 2. These values are almost in agreement with reported values for other perovskite manganites[27, 55]. It is obseravable in Table 2 that the γ_p value increases from 5.83 to 8.05 by increasing sintering temperature from 800 ˚C to 1350 ˚C. It is interpreted that $\gamma_p > 4$ exhibits strong electron-phonon interaction in manganites. It is also remarkable to note that $\frac{m_p}{m^*}$ value increases for S1350 sample compared with S800 sample. The large values of γ_p and $\frac{m_p}{m^*}$ for samples indicate strong electron-phonon interaction in these systems which also supports the formation of small polaron. Also it can be concluded that the electron-phonon interaction in S1350 sample is stronger in comparison to S800 sample.

3.3.2. $T<\Theta_D/2$: Variable Range Hopping (VRH) model

When the carriers are localized near the Fermi energy by random potential fluctuation, as is in the case of hole-doped manganites, the resistivity data can be studied by Mott's variable range hopping (VRH) model. In this model, the conduction mechanism is interpreted on the basis of electron hopping. A hopping electron will always try to find the lowest activation energy and the shortest hopping distance. However, usually the two conditions cannot be satisfied at the same time. So, there will be an optimum hopping distance, which maximizes the hopping probability. As a matter of fact, in this temperature region, the electrons don't hop to the nearest neighbors, so the electron hopping is variable range type which can be expressed as [56, 57]:

$$\boldsymbol{\rho} = \boldsymbol{\rho_0}\ \mathbf{exp}\left(\frac{T_0}{T}\right)^{\frac{1}{p}} \quad (7)$$

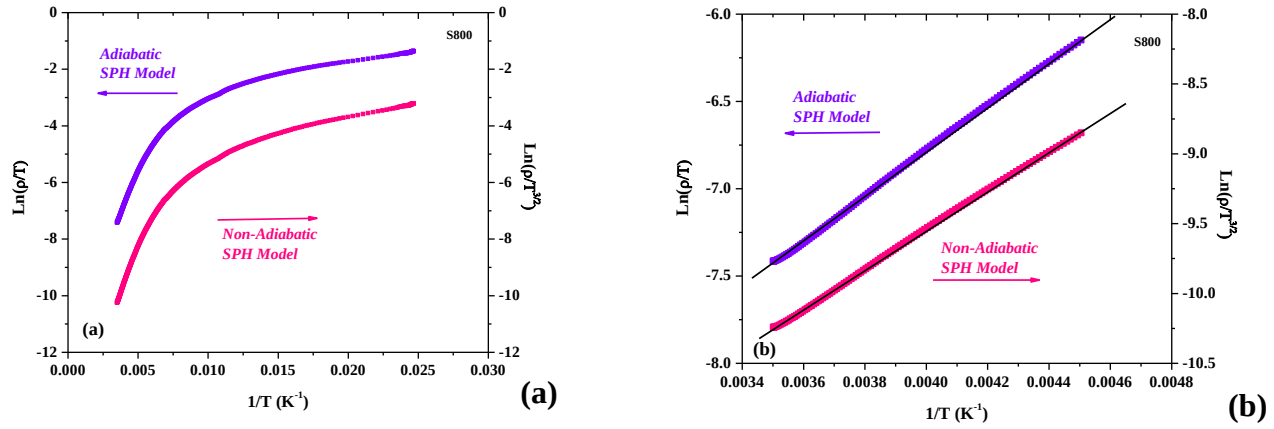

Fig. 7. Plots of Ln(ρ/T) and Ln(ρ/$T^{3/2}$) versus (1/T) for S800 sample (a) in all temperature ranges and (b) above 222 K.

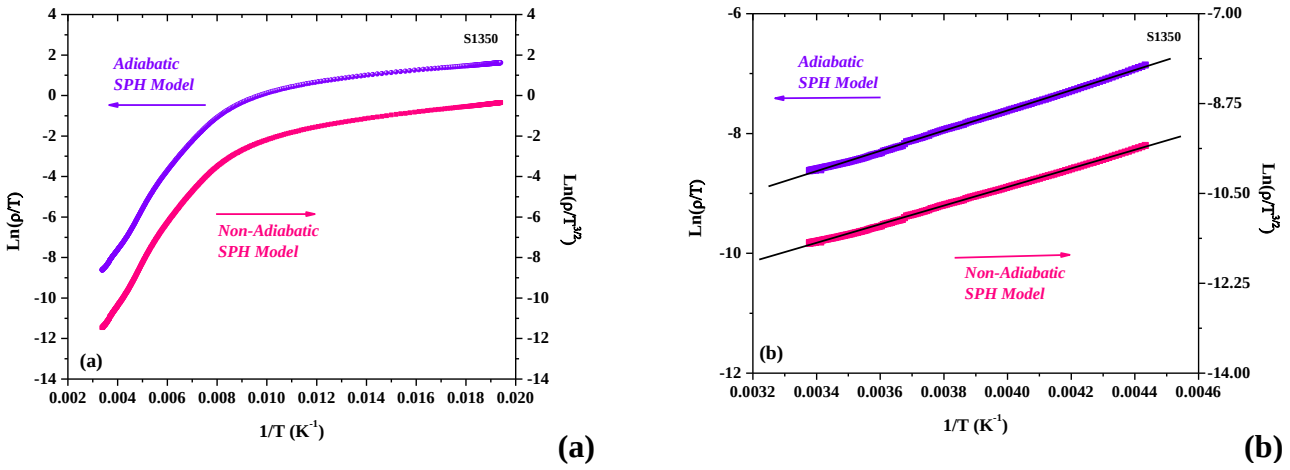

Fig. 8. Plots of Ln(ρ/T) and Ln(ρ/$T^{3/2}$) versus (1/T) for S1350 sample (a) in all temperature ranges and (b) above 225 K.

Table 1.Calculated parameters from resistivity data of S800 and S1350 samples fitted with adiabatic and non-adiabatic SPH models.

	Adiabatic SPH			***Non-adiabatic SPH***		
Sample	**R^2**	**ρ_α(ΩCmK^{-1})**	**E_a (meV)**	**R^2**	**ρ_α(ΩCmK^{-1})**	**E_a (meV)**
S800	0.9996	6.41×10^{-6}	111.53	0.9996	2.41×10^{-7}	122.67
S1350	0.9987	5.99×10^{-7}	144.65	0.9989	2.22×10^{-8}	156.09

Table 2. Parameters evaluated using Eqs. (3-6).

Sample	Ø (meV)	J (meV)	γ_p	m_p/m^*
S800	22.86	23.25	5.83	340.36
S1350	24.55	23.48	8.05	3133.79

Where $\boldsymbol{p} = \frac{1}{d+1}$ depends on the dimensionality of the system.

In 3-dimensional conductance, the expression for resistivity in this model has the form[58]:

$$\boldsymbol{\rho = \rho_0 \exp\left(\frac{T_0}{T}\right)^{\frac{1}{4}}} \quad (8)$$

Where T_0 is the expression for Mott's activation energy and is given by [29, 53, 55]:

$$\boldsymbol{K_B T_0 = \frac{16\alpha^3}{N(E_F)}} \quad (9)$$

Where $N(E_F)$ is the density of state (DOS) at the Fermi level, K_B is the Boltzmann's constant and α is related to the localization length.

Table 3. Extracted parameters from resistivity data of S800 and S1350 samples fitted with VRH model.

	3-Demenstional VRH			
Sample	**R^2**	**ρ_0 (ΩCm)**	**T_0 (K)**	**$N(E_f)(eV^{-1}Cm^{-3})$**
S800	0.9999	2.39×10^{-8}	1.77×10^{7}	1.29×10^{20}
S1350	0.9996	6.09×10^{-18}	4.79×10^{8}	4.77×10^{18}

According to Eq. 8, a fit was made between resistivity and temperature below $\Theta_D/2$ and the results are shown in the inset of Figures 9 and 10. The fitting parameters are tabulated in Table 3. R^2 values indicate relativity well correlation coefficient for both samples and it can be concluded that both samples follow VRH model in the temperature region of $T< \Theta_D/2$. It is to be noted that the obtained value of T_0 for S1350 sample is larger than corresponding value for S800 sample. This could be due to the reduction of $N(E_F)$ (according to Eq. 9). If we estimate α=2.22 nm^{-1} [27, 49, 57], the $N(E_F)$ values can be calculated from the obtained T_0 values. The $N(E_F)$ values are calculated and listed in Table 3. These values are comparable to corresponding values of other manganites [26, 27]. As a matter of fact, when the conduction is reduced, more activation energy is needed for carrier hopping and consequently, $N(E_F)$ decreases.

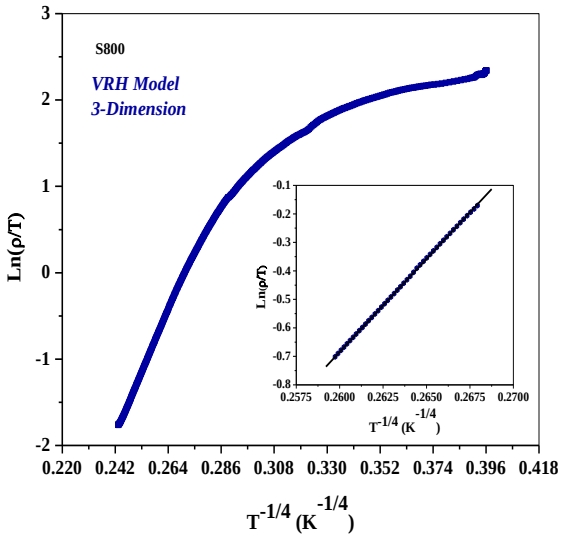

Fig. 9. Ln(ρ/T) versus (1/T) plot for S800 sample. The inset shows the fit of resistivity to VRH model.

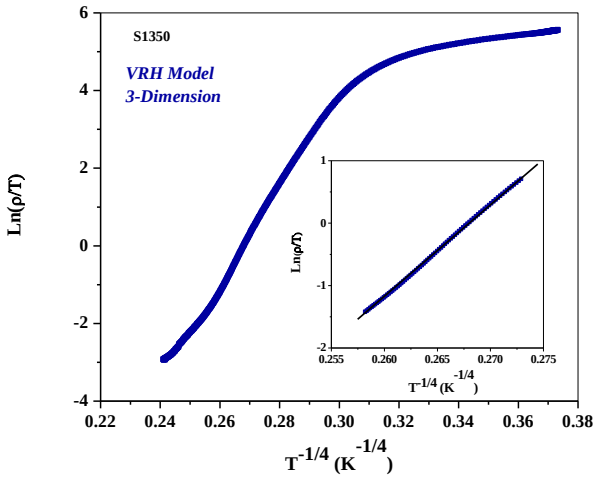

Fig. 10. Ln (ρ/T) versus (1/T) plot for S1350 sample. The inset shows the fit of resistivity to VRH model.

4. Conclusion

The structural, magnetic, and electrical transport properties of phase separated $La_{0.5}Ca_{0.5}MnO_3$ manganite with two different particle sizes have been studied. The XRD data show an orthorhombic structure with P*nma* space group for both samples with different particle sizes and no structural transition is observed by increasing particle size. Magnetic study indicates that the AFM phase is enhanced with increasing sintering temperature. So that, bulk sample shows thermal hysteresis which is due to the phase separation. Electrical studies revealed that both samples behave like an insulator. The electrical behavior investigation based on polaronic transport models shows the obvious difference in resistivity patterns of samples. At $T>\Theta_D/2$, the resistivity data of nanometer sized sample follow the adiabatic SPH model, while those of bulk sample follows the non-adiabatic SPH model. Also, it has been found that 3-dementional VRH model can describe the conduction mechanism of both samples at $T<\Theta_D/2$ region. The parameters are extracted by analyzing the data with SPH and VRH models and the effect of particle size on these parameters is investigated.

References

[1] G.H. Jonker, J.H. Van Santen. "Ferromagnetic compounds of manganese with perovskite structure." Physica 16 (1950) 337-349.

[2] B.P. McCarthy, L.R. Pederson, Y.S. Chou, X.D. Zhou, W.A. Surdoval, L.C. Wilson, "Low-temperature sintering of lanthanum strontium manganite-based contact pastes for SOFCs." Journal of power sources 180 (2008) 294-300.

[3] Shuaizhao Jin, Xin Gu, Xiaohan Yu, Xiaoli Guan, Yixin Yan, Kaikai Wu, Liming Zhao, Yan Zhu, Shuhong Sun, Jinkun Liu, Jin Hu, Jun Zhao, Lingde Kong, Wenyun Yang, Qingming Chen, Parviz Kameli, Xiang Liu, "Adjusting the K-doping of La1-xKxMnO3 (0.1≤ x≤ 0.35) films to obtain high TCR and LFMR at room-temperature." Applied Surface Science 589 (2022)152905.

[4] Tina Raoufi, Ali Ghotbi Varzaneh, Mohammad Hossein Ehsani, Enke Liu, Volodymyr Chernenko, "Tuning magnetic and table-like magnetocaloric effect of La0. 6− xErxSr0. 4MnO3 (x= 0.0125, 0.05, 0.1) manganites." Materials Research Bulletin 156(2022) 111997.

[5] P. Amirzadeh, H. Ahmadvand, P. Kameli, B. Aslibeiki, H. Salamati, A. Gamzatov, A. Aliev, I. Kamilov, "Phase separation and direct magnetocaloric effect in La 0.5 Ca 0.5 MnO 3 manganite." Journal of Applied Physics 113 (2013) 123904.

[6] P. Levy, F. Parisi, G. Polla, D. Vega, G. Leyva, H. Lanza, R.S. Freitas, L. Ghivelder, "Controlled phase separation in La 0.5 Ca 0.5 MnO 3." Physical Review B 62 (2000) 6437.

[7] F. Parisi, P. Levy, G. Polla, D. Vega, G. Leyva, H. Lanza, R.S. Freitas, L. Ghivelder, "Phase separation in La0. 5Ca0. 5MnO3 controlled trough thermal treatments." Journal of magnetism and magnetic materials 226, (2001) 1901-1903.

[8] P.G. Radaelli, D.E. Cox, M. Marezio, S.W. Cheong, "Charge, orbital, and magnetic ordering in La 0.5 Ca 0.5 MnO 3 s." Physical Review B 55 (1997) 3015.

[9] V.P.S. Awana, R. Tripathi, S. Balamurugan, A. Kumar, A. Dogra, H. Kishan, "Thermal hysteresis in electrical transport of charge ordered La0. 5Ca0. 5MnO3 manganites." Journal of alloys and compounds 475 (2009) L13-16.

[10] J. van den Brink, G. Khaliullin, D. Khomskii, "Charge and orbital order in half-doped manganites." Physical review letters 83 (1999) 5118.

[11] M. Zarifi, P. Kameli, A. Ghotbi Varzaneh, E. Hosseini, M. Norouzi-Inallu, M. Abbasi Eskandari, H. Ahmadvand, "Anisotropic resistivity and electroresistance in epitaxial La0. 3Pr0. 4Ca0. 3MnO3 thin films." Applied Physics *A* 128 (2022) 1-8.

[12] T. Sarkar, B. Ghosh, A.K. Raychaudhuri, T. Chatterji, "Crystal structure and physical properties of half-doped manganite nanocrystals of less than 100-nm size." Physical Review B 77 (2008) 235112.

[13] M. Oumezzine, O. Peña, T. Guizouarn, R. Lebullenger, M. Oumezzine, "Impact of the sintering temperature on the structural, magnetic and electrical transport properties of doped La0, 67Ba0, 33Mn0, 9Cr0, 1O3 manganite." Journal of magnetism and magnetic materials 324 (2012) 2821-2828.

[14] D.H. Manh, P.T. Phong, T.D. Thanh, L.V. Hong, N.X. Phuc, "La0. 7Ca0. 3MnO3 perovskite synthesized by reactive milling method: The effect of particle size on the magnetic and electrical properties." Journal of alloys and compounds 491 (2010) 8-12.

[15] D.G. Kuberkar, R.R. Doshi, P.S. Solanki, U. Khachar, M. Vagadia, A. Ravalia, V. Ganesan, "Grain morphology and size disorder effect on the transport and magnetotransport in sol–gel grown nanostructured manganites." Applied Surface Science 258 (2012) 9041-9046.

[16] P. Dey, T.K. Nath, "Effect of grain size modulation on the magneto-and electronic-transport properties of La 0.7 Ca 0.3 Mn O 3 nanoparticles: The role of spin-polarized tunneling at the enhanced grain surface." Physical Review B 73 (2006) 214425.

[17] S. Roy, I. Dubenko, D.D. Edorh, N. Ali, "Size induced variations in structural and magnetic properties of double exchange La 0.8 Sr 0.2 MnO 3− δ nano-ferromagnet." Journal of applied physics 96 (2004) 1202-1208.

[18] P. Siwach, U. Goutam, P. Srivastava, H. Singh, R. Tiwari, O. Srivastava, "Colossal magnetoresistance study in nanophasic La0. 7Ca0. 3MnO3 manganite." Journal of Physics D: Applied Physics 39 (2006) 14.

[19] M.H. Ehsani, P. Kameli, M.E. Ghazi, "Influence of grain size on the electrical properties of the double-layered LaSr2Mn2O7 manganite." Journal of Physics and Chemistry of Solids 73 (2012) 744.

[20] E.O. Wollan, W.C. Koehler, "Neutron diffraction study of the magnetic properties of the series of perovskite-type Compounds [(1− x) La, x Ca] Mn O 3." Physical Review 100 (1955) 545.

[21] J.B. Goodenough, "Theory of the role of covalence in the perovskite-type manganites [La, M (II)] Mn O 3." Physical Review 100 (1955) 564.

[22] R. Kajimoto, T. Kakeshita, Y. Oohara, H. Yoshizawa, Y. Tomioka, Y. Tokura, "Anomalous ferromagnetic spin fluctuations in an antiferromagnetic insulator Pr 1− x Ca x MnO 3." Physical Review B 58 (1998) R11837.

[23] S. Yunoki, T. Hotta, E. Dagotto, "Ferromagnetic, A-type, and charge-ordered CE-type states in doped manganites using Jahn-Teller phonons." Physical review letters 84 (2000) 3714.

[24] T. Mizokawa, D.I. Khomskii, G.A. Sawatzky, "Orbital polarons and ferromagnetic insulators in manganites." Physical Review B 63 (2000) 024403.

[25] B.J. Campbell, S.K. Sinha, R. Osborn, S. Rosenkranz, J.F. Mitchell, D.N. Argyriou, L. Vasiliu-Doloc, O.H. Seeck, J.W. Lynn, "Polaronic orbital polarization in a layered colossal magnetoresistive manganite." Physical Review B 67 (2003) 020409.

[26] S. Mollah, H.L. Huang, H.D. Yang, S. Pal, S. Taran, B.K. Chaudhuri, "Non-adiabatic small-polaron hopping conduction in Pr0. 65Ca0. 35− xSrxMnO3 perovskites above the metal–insulator transition temperature." Journal of magnetism and magnetic materials 284 (2004) 383-394.

[27] S. Mollah, Z.A. Khan, D.K. Shukla, M. Arshad, R. Kumar, A. Das, "Adiabatic small polaron-hopping conduction in Ln0. 85Ca0. 15MnO3 (Ln= Nd, Pr and Sm) perovskites." Journal of Physics and Chemistry of Solids 69 (2008) 1023-1028.

[28] M.F. Mostafa, S.S. Ata-Allah, A.A.A. Youssef, H.S. Refai, "Electric and AC magnetic investigation of the manganites La0. 7Ca0. 3Mn0. 96In0. 04xAl (1− x) 0.04 O3;(0.0⩽ x⩽ 1.0)." Journal of magnetism and magnetic materials 320 (2008) 344-353.

[29] G. Venkataiah, D.C. Krishna, M. Vithal, S.S. Rao, S.V. Bhat, V. Prasad, S.V. Subramanyam, P.V. Reddy, "Effect of sintering temperature on electrical transport properties of La0. 67Ca0. 33MnO3." Physica B: Condensed Matter 357 (2005) 370-379.

[30] J. Rodríguez-Carvajal, "11 April 2017." Physica B 192 (1993) 55-69.

[31] R.S. Freitas, L. Ghivelder, P. Levy, F. Parisi, "Magnetization studies of phase separation in La 0.5 Ca 0.5 MnO 3." Physical Review B 65 (2002) 104403.

[32] E. Rozenberg, M. Tsindlekht, I. Felner, E. Sominski, A. Gedanken, Y.M. Mukovskii, C.E. Lee, "Size and Nonstoichiometry Effects on Magnetic Properties of ${\hbox {La}} _ {0.5}\hbox {Ca} _ {0.5}\hbox {MnO} _ {3} $ Manganite." IEEE transactions on magnetics 45 (2009) 2576-2579.

[33] Z. Jirák, E. Hadová, O. Kaman, K. Knížek, M. Maryško, E. Pollert, M. Dlouhá, S. Vratislav, "Ferromagnetism versus charge ordering in the Pr 0.5 Ca 0.5 MnO 3 and La 0.5 Ca 0.5 MnO 3 nanocrystals." Physical Review B 81 (2010) 024403.

[34] R.N. Bhowmik, R. Nagarajan, R. Ranganathan, "Magnetic enhancement in antiferromagnetic nanoparticle of CoRh 2 O 4." Physical Review B 69 (2004) 054430.

[35] A. Pramanik, A. Banerjee, "Phase separation and the effect of quenched disorder in Pr0. 5Sr0. 5MnO3." Journal of Physics: Condensed Matter 20 (2008) 275207.

[36] S.B. Roy, "First order magneto-structural phase transition and associated multi-functional properties in magnetic solids." Journal of Physics: Condensed Matter 25 (2013) 183201.

[37] J. Fan, B. Hong, Y. Ying, L. Ling, L. Pi, Y. Zhang, "Strain-driven inverse thermal hysteresis behaviour in half-doped manganites." Journal of Physics D: Applied Physics 41 (2008) 105013.

[38] V. Markovich, I. Fita, R. Puzniak, C. Martin, A. Wisniewski, C. Yaicle, A. Maignan, G. Gorodetsky, "Instability of magnetism in Pr 0.5 Ca 0.5 Mn 1− x Cr x O 3 (x= 0.015, 0.03): Competition between pressure and thermal cycling effects." Physical Review B 73 (2006) 224423.

[39] A. Levanyuk, A.S. Sigov, "Defects and structural phase transitions." Gordon and Breach Science Publishers, (1988).

[40] R. Mahendiran, A. Maignan, M. Hervieu, C. Martin, B. Raveau, "Spectacular increase of resistivity by thermal cycling under a magnetic field in Pr0. 5Ca0. 5Mn0. 99Cr0. 01O3." Journal of Solid State Chemistry 160 (2001) 1-3.

[41] L. Pi, J. Cai, Q. Zhang, S. Tan, Y. Zhang, "Training effect by the applied magnetic field in the double-doped Pr 0.5+ 0.5 x Ca 0.5− 0.5 x Mn 1− x Cr x O 3 system." Physical Review B 71 (2005) 134418.

[42] M. Eshraghi, H. Salamati, P. Kameli, "Structural, magnetic and transport properties of La0. 8Sr0. 2MnO3/xNiO composites." Journal of Physics: Condensed Matter 18 (2006) 8281.

[43] D. Das, C. Srivastava, D. Bahadur, A. Nigam, S. Malik, "Magnetic and electrical transport properties of La0. 67Ca0. 33MnO3 (LCMO): xZnO composites." Journal of Physics: Condensed Matter 16 (2004) 4089.

[44] M. Rubinstein, "Two-component model of polaronic transport." Journal of Applied Physics 87 (2000) 5019-5021.

[45] A. Gaur, G. Varma, "Sintering temperature effect on electrical transport and magnetoresistance of nanophasic La0. 7Sr0. 3MnO3." Journal of Physics: Condensed Matter 18 (2006) 8837.

[46] D. Worledge, G.J. Snyder, M. Beasley, T. Geballe, R. Hiskes, S. DiCarolis, "Anneal-tunable Curie temperature and transport of La0. 67Ca0. 33MnO3." Journal of applied physics 80 (1996) 5158-5161.

[47] D. Emin, T. Holstein, "Studies of small-polaron motion IV. Adiabatic theory of the Hall effect." Annals of Physics 53 (1969) 439-520.

[48] J. Appel, "Polarons." Solid State Physics 21 (1968) 193-391.

[49] A. Banerjee, S. Pal, B.K. Chaudhuri, "Nature of small-polaron hopping conduction and the effect of Cr doping on the transport properties of rare-earth manganite La 0.5 Pb 0.5 Mn 1− x Cr x O 3." The Journal of Chemical Physics 115 (2001) 1550-1558.

[50] A. Banerjee, S. Pal, S. Bhattacharya, B.K. Chaudhuri, H.D. Yang, "Particle size and magnetic field dependent resistivity and thermoelectric power of La 0.5 Pb 0.5 MnO 3 above and below metal–insulator transition." Journal of applied physics 91 (2002) 5125-5134.

[51] T. Holstein, "Studies of polaron motion: Part II. The "small" polaron." Annals of physics 8 (1959) 343-389.

[52] M. Ehsani, P. Kameli, F. Razavi, M. Ghazi, B. Aslibeiki, "Influence of Sm-doping on the structural, magnetic, and electrical properties of La0. 8− xSmxSr0. 2MnO3 (0< x< 0.45) manganites." Journal of alloys and compounds 579 (2013) 406-414.

[53] I. Austin, "Polarons in crystalline and non-crystalline materials." Advances in physics 18 (1969) 41-102.

[54] N.F. Mott, "Conduction in glasses containing transition metal ions." Journal of Non-Crystalline Solids 1 (1968) 1-7.

[55] W.H. Jung, "Adiabatic small polaron hopping conduction in La0. 7Nd0. 3Mn0. 8Cr0. 2O3." Physica B: Condensed Matter 404 (2009) 1953-1956.

[56] B.I. Shklovskii, "Hopping conduction in lightly doped semiconductors." Sov Phys Semicond 6 (1973) 1053-1075.

[57] M. Viret, L. Ranno, J.M.D. Coey, " Magnetic localization in mixed-valence manganites." Physical Review B 55 (1997) 8067.

[58] N.F. Mott, E.A. Davis, "Electronic processes in non-crystalline materials." Oxford University Press, 2012.